Dynamics of a self-avoiding polymer chain in slit, tube, and cube confinements

Ting Cui,[1] Jiandong Ding,[1,*] and Jeff Z. Y. Chen[2,†]
[1]*Key Laboratory of Molecular Engineering of Polymers of Ministry of Education, Department of Macromolecular Science, Advanced Materials Laboratory, Fudan University, Shanghai 200433, China*
[2]*Department of Physics and Astronomy, University of Waterloo, Waterloo, Ontario, Canada N2L 3G1*
(Received 29 August 2008; published 29 December 2008)

Monte Carlo simulations are presented for the observation of the dynamics of a self-avoiding polymer in three types of confinement: slit, tube, and cube. We pay special attention to the parameter regime where the characteristic confinement dimension is smaller than the radius of gyration of the unconfined polymer. On the basis of the bond-fluctuation model, we measured the rotation time of the end-to-end vector of the polymer, the diffusion time for the center of the polymer to move a distance comparable to the root mean square end-to-end distance, and the looping time for the ends of the polymer to approach each other from an open position. As functions of the confinement width and polymer length, these three time scales are discussed in light of scaling theories.

DOI: 10.1103/PhysRevE.78.061802 PACS number(s): 82.35.Lr, 36.20.Ey, 02.70.Uu

I. INTRODUCTION

The conformational properties of a self-avoiding polymer coil confined in a slit or in a cylindrical tube, formed by impenetrable walls, are now relatively well understood. The dependence of the free energy and the confined polymer's size on the length of the polymer and confinement width in such systems can be well described by the scaling arguments of de Gennes [1,2]. Although relatively simple, these models have captured the general physical properties of an enormously wide range of practical systems, guiding our understanding of polymer and biological systems.

The interest in thoroughly understanding various dynamic processes of a self-avoiding polymer confined by various types of geometries can be related to their applicability in many synthetic and natural polymer systems. In this paper, using Monte Carlo simulations, we discuss the characteristic times associated with a few typical dynamic processes of a polymer confined in a slit formed by two flat walls, a square tube formed by four flat walls, and a cubic pore formed by six rigid walls (see Fig. 1). These theoretical models serve as the basis for practical applications in chemical and biological systems. For example, when polymer chains react in highly dispersed media such as micelles, mesophases, or microemulsion droplets, each chain occupies its own microcompartment, where its static and dynamic behaviors are expected to be strongly influenced by the confinement. In another example, the effects of spatial confinement (e.g., ribosomes) and macromolecular crowding (e.g., molecular chaperones) have been suggested as one of the main reasons that can significantly influence protein folding rates and the stability of the folded state [3–6]. Because of the recent advance in experimental techniques, the static and dynamic behavior of a single biological molecule in a confining environment can now be directly probed [7–11].

The dynamical properties of a polymer chain confined in a *slit* confinement were considered by Brochard and de Gennes in a scaling analysis with the excluded volume effects incorporated [12]. Indeed, in the strong confinement limit the dynamical properties were found to be in full agreement with the Rouse model with excluded volume in two dimensions [13–16]. In agreement with previous studies [1,2,12–16], in this paper we show that the measured dynamic properties of a self-avoiding polymer in strong slit confinement can be mostly captured by the rotation relaxation time τ_{rot} of the end-to-end vector. We demonstrate that, for example, the diffusion time for a polymer to move a

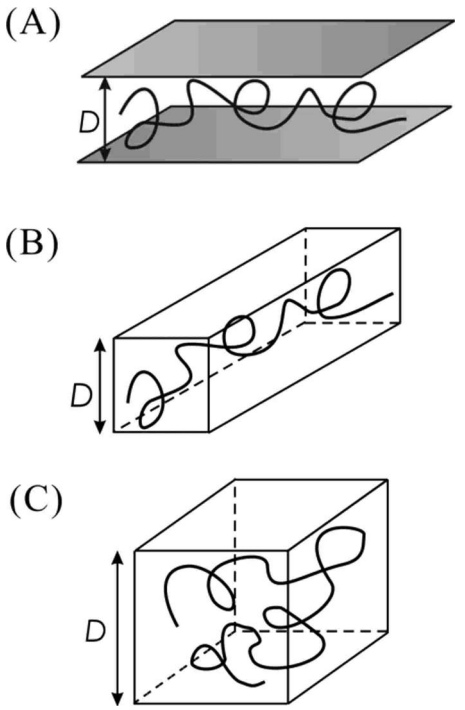

FIG. 1. Schematic representation of a self-avoiding polymer confined in (a) a slit formed by two parallel hard walls with a separation D, (b) a square tube formed by four parallel walls with a square cross section of area D^2, and (c) a cubic pore formed by six parallel walls with a volume of D^3.

*Corresponding author. jdding1@fudan.edu.cn
†Corresponding author. jeffchen@uwaterloo.ca

distance equivalent to the size of a polymer, τ_{diff}, is proportional to τ_{rot}; as well, the looping time for the two ends of the polymer to approach each other within a distance of the order of the bond length from an equilibrium open position, τ_{loop}, is also proportional to τ_{rot}.

More recent attentions have been paid to the dynamical properties of a polymer chain confined in a *tube* confinement [17–20]. In the strong tube confinement limit, where the tube diameter is smaller than the radius of gyration of the free space polymer, however, the above-mentioned time scales do not necessarily agree with each other for a self-avoiding chain. Unlike the case of a polymer confined in a slit, the dynamic times are more complicated and depend on the dynamic properties that are under observation. Avramova and Milchev have confirmed that the diffusion time for the polymer to move from its original position to a distance equivalent to its elongated size along the tube axis is proportional to N^3, where N is the number of bonds in the chain [17]. Our simulation results in this work confirm the scaling relationship observed by Avramova and Milchev and, in addition, as one of our results, we verify that the dependence on the dimension of the cross section of the confinement is fully consistent with a scaling argument as well. Furthermore, we explore the rotation time of the end-to-end vector and convincingly show that the rotational time follows an exponential scaling behavior, in agreement with a recent suggestion of Huang and Makarov [20]. Inspired by a number of biological phenomena, we have also measured the looping time for the two ends of the polymer to approach each other, which also displays an exponential law similar to the rotational time in the strong confinement limit.

The physical properties of a self-avoiding polymer confined in a cavity are usually connected to a number of actual examples in synthetic and biological polymer systems. For intrachain polymer looping under confinement of a spherical geometry, it has been shown that an optimal confinement size exists where the looping is fastest [21,22]. In this work our simulation results for a self-avoiding polymer in a *cubic* pore verify the existence of a relaxation time minimum; our data and our scaling argument suggest that, for a polymer of length N, the optimal pore size for relaxation of polymer is proportional to $N^{1/3}$.

The computer simulations performed in this work are based on an implementation of the bond-fluctuation model, effectively mimicking the Brownian dynamics of a polymer chain [23,24]. In this model, the excluded volume interaction between monomers is ensured and no bond crossing is permitted. The model has been commonly used in other studies for understanding the basic dynamic properties of polymers [25–29].

We describe the Monte Carlo simulation used in this work and technical details on the measurement of dynamic times in Sec. II; readers can directly skip to Sec. III for the main results and discussion of the scaling behavior.

II. SIMULATION METHOD

In the bond-fluctuation model, the excluded volume interaction between monomers is ensured and no bond crossing is permitted. The systems are embedded in a cubic square lattice with a unit cell size l. In a trial move, a monomer is displaced in a random direction by an allowed distance from the original position; the move is accepted only if the new position is unoccupied [23,24]. The dynamic properties of the polymers are reproduced with the understanding that the diffusive motion of monomers can be effectively modeled by a Monte Carlo procedure, in a system where the hydrodynamic effects are ignored [30,31].

Our implementation of the bond-fluctuation model contained additional constraints beyond the commonly used bond-fluctuation moves; the systems were subject to hard boundary conditions for the simulation of hard-wall confinements. Any trial move that made the monomer cross a hard wall was rejected. We considered three different types of confinement in this work. (a) For the slit confinement, the system contains two parallel walls located at $z=\pm D/2$ which extend infinitely along the x and y axes, where D is the slit width. (b) For the square-tube confinement, the system contains a tube axis coinciding with the z axis and the motion of the polymer was restricted to the interior of four walls located at $x=\pm D/2$ and $y=\pm D/2$, where D is the tube width. (c) Finally, for the cubic confinement, the polymer is allowed to move inside a cubic volume bounded by six hard walls, $x=\pm D/2$, $y=\pm D/2$, and $z=\pm D/2$, where D is the cube dimension.

The initial polymer configuration was created to observe the presence of the hard-wall confinement within the framework of the bond-fluctuation model. Whenever possible, we randomly placed monomers along the chain to generate the preliminary configuration of a chain formed by N monomers, each occupying a cubic lattice cell measuring $2l\times 2l\times 2l$ on a cubic lattice in three dimensions. However, in the strong confinement limit, in particular for the cubic confinement, we have lifted the excluded volume constraint for the initial generation of the configurations; a configuration containing monomer overlapping was then subject to a prepared Monte Carlo run that is biased to removal of the overlapping. Once all overlapping is removed, we obtain a preliminary configuration that contains $N+1$ nonoverlapping monomers.

The preliminary configuration was then subject to a sufficiently long equilibration period of relaxation following the standard bond-fluctuation algorithm. Adopting the unit that a Monte Carlo step (MCS) corresponds to $N+1$ attempts at moving randomly selected monomers, for the equilibration period we used at least 20 times the relaxation time of an unconfined self-avoiding polymer of N bonds, determined within the same bond-fluctuation model (see Fig. 2).

For every set of parameters D and N, we followed the Monte Carlo dynamics and calculated three characteristic time scales that will be discussed below: the rotational relaxation time τ_{rot} of the end-to-end vector, the mean first-passage time τ_{loop} of looping events where the two terminal monomers approach each other and make contact from equilibrated open configurations, and the diffusion time τ_{diff} of the diffusive displacement of the entire chain to a distance equal to the root mean square end-to-end distance.

The definition of the rotational relaxation time was based on the calculation of the autocorrelation function of the end-to-end distance vector $\mathbf{R}(t)$ at Monte Carlo time t,

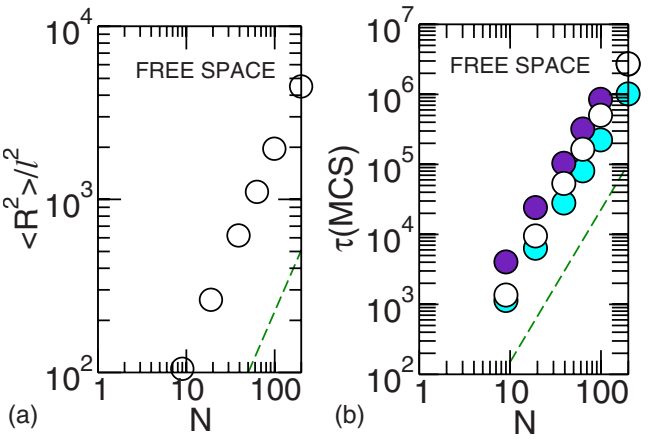

FIG. 2. (Color online) (a) Mean square end-to-end distance and (b) the three dynamic times measured in this work for a self-avoiding polymer in free space as a function of the number of bonds N. In (b), open, dark (purple online), and gray (cyan online) symbols correspond to looping time τ_{loop}, diffusion time τ_{diff}, and rotation time τ_{rot}, respectively. The dashed lines (green online) in (a) and (b) indicate slopes of 2ν and $1+2\nu$ (ν=0.588), for the expected scaling exponents of the mean square end-to-end distance and Rouse dynamic time.

$$c(t) = \langle \mathbf{R}(t) \cdot \mathbf{R}(0) \rangle / \langle R^2 \rangle, \tag{1}$$

where $\langle R^2 \rangle$ is the mean square end-to-end distance. We performed the ensemble average $\langle \cdots \rangle$ on the basis of data collected from 200 independent production runs. The calculated $c(t)$ has a typical exponential decaying behavior; the measured negative slope determines the inverse rotational time, $1/\tau_{\text{rot}}$.

The diffusion time was determined from the mean square displacement of the center of mass of the polymer,

$$G(t) = \langle [\mathbf{R}_{\text{c.m.}}(t) - \mathbf{R}_{\text{c.m.}}(0)]^2 \rangle, \tag{2}$$

where $\mathbf{R}_{\text{c.m.}}(t)$ is the coordinate of the center of mass at time t. The ensemble average $\langle \cdots \rangle$ is based on data collected from 200 independent production runs and $G(t)$ typically shows a linear dependence on t. The diffusion time for the polymer to move out of its original position, τ_{diff}, was then numerically obtained from $G(t)$ by enforcing

$$G(\tau_{\text{diff}}) = \langle R^2 \rangle. \tag{3}$$

Both τ_{rot} and τ_{diff} were produced from the same series of production runs.

The looping time τ_{loop} was produced from another set of simulations. We directly monitored the configuration fluctuations of the polymer after an adequate relaxation period to ensure equilibration. An arbitrary open polymer configuration was adopted and the time duration for the two ends to reach a specified distance of $3l$ was recorded, where l is the lattice constant of the embedded square lattice in the bond-fluctuation model [23,24]. An average of 10^3 independent measurements of the looping time gives us the mean, τ_{loop}. We have adopted a relatively large capture radius of $3l$; in such a case the looping time of a free space polymer follows almost the same power law as the rotational time of the end-to-end vector [32].

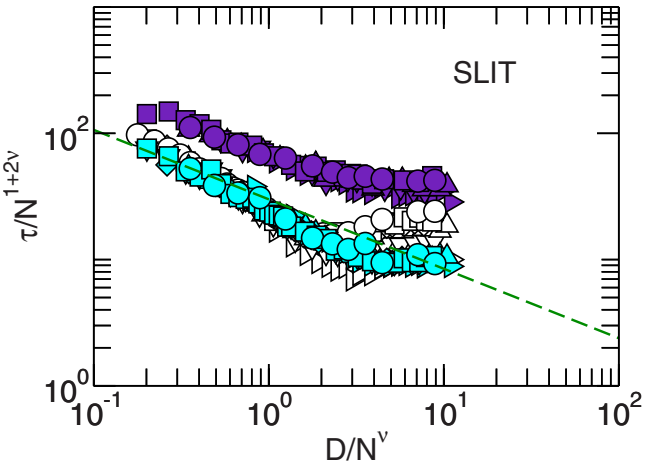

FIG. 3. (Color online) Reduced dynamic time scales as a function of D/N^{ν}, for a self-avoiding polymer confined in a slit with a wall-to-wall distance of D. Open, light gray (cyan online), and dark gray (purple online) symbols represent the looping time, rotation time, and diffusion time, respectively. The dashed straight line is an indication of a slope of −0.55 in this logarithmic plot. Circles, squares, diamonds, up triangles, down triangles, and right triangles correspond to polymer chain lengths (the number of bonds) N =199, 99, 63, 39, 19, and 9.

Before we turn to the discussion of the results, in Fig. 2(a) we show that our simulation data for the mean square end-to-end distance of a free-space polymer follow the expected scaling behavior,

$$\langle R^2(N, D=\infty) \rangle \propto N^{2\nu}, \tag{4}$$

where ν is the scaling exponent ν=0.588… [33]. Both τ_{rot} and τ_{diff} are seen to follow the Rouse time,

$$\tau_{\text{rot}}(N, D=\infty) \propto \tau_{\text{diff}}(N, D=\infty) \propto \tau_{\text{Rouse}} \propto N^{1+2\nu}. \tag{5}$$

Theoretically, τ_{loop} would follow a similar power law but might have a slightly different numerical value for the scaling exponent; within the range of N and the numerical accuracy of our simulation, the data for τ_{loop} in Fig. 2 can also be described numerically by the same scaling behavior.

III. RESULTS AND DISCUSSION

A. Slit confinement

In Fig. 3, the measured rotational relaxation time τ_{rot} as a function of N and D is shown by light gray symbols, plotted in a reduced form as a function of D/N^{ν}, where ν=0.588 is the scaling exponent for the radius of gyration of a polymer in a good solvent. In this figure, the data points for $\tau_{\text{rot}}(N,D)/N^{1+2\nu}$ collapse into a universal curve, suggesting that it is a function of a single reduced variable D/N^{ν}:

$$\tau_{\text{rot}}(N,D)/N^{1+2\nu} = f(D/N^{\nu}), \tag{6}$$

rather than two independent variables N and D. A significant feature of the plot in Fig. 3 is the power-law behavior of the

light and dark gray symbols in the small D/N^{ν} limit where our data points converge to a slope close to $-1/2$ (the dotted line in Fig. 3).

To dissect the polymer dynamics in the strong confinement regime, we first consider the diffusion time for the polymer to move in the x and y directions to a position that does not overlap the original. The polymer can freely rotate and diffuse in the x and y directions under the slit confinement, in analogy to the motion of a two-dimensional polymer. Taking the definition of τ_{diff} from Eq. (3) and the fact that $G_{\mathrm{c.m.}}(t) \propto D_0 t$ where D_0 is the diffusion constant, we can write

$$\tau_{\mathrm{diff}}(N,D) \propto \langle \mathbf{R}_{\parallel}^2 \rangle / D_0, \tag{7}$$

where $\langle \mathbf{R}_{\parallel}^2 \rangle$ is the average square end-to-end distance in the x- and y-directions. Then, taking the scaling behavior of $\langle \mathbf{R}_{\parallel}^2 \rangle$ [34],

$$\langle \mathbf{R}_{\parallel}^2 \rangle / N^{2\nu} \propto (N^{\nu}/D)^{2\nu_2/\nu - 2}, \tag{8}$$

and $D_0 \propto 1/N$ (generally regarded as valid for the diffusion of a polymer in the freely draining limit) [35], we have

$$\tau_{\mathrm{diff}}(N,D)/N^{1+2\nu} \propto (N^{\nu}/D)^{2\nu_2/\nu - 2}, \tag{9}$$

where $\nu_2 = 3/4$ is the exact scaling exponent for the polymer size of a two-dimensional self-avoiding polymer [36].

Now, for the case of a strong slit confinement, we expect $\tau_{\mathrm{diff}}(N,D) \propto \tau_{\mathrm{rot}}(N,D)$ for small D/N^{ν}. Hence, the universal function $f(x)$ in Eq. (6) follows an asymptotic power law $x^{-(2\nu_2/\nu - 2)} = x^{-0.55\cdots}$ in the small x regime. The observed convergence of light and dark gray data points to a slope of -0.55 in the double-logarithmic plot in Fig. 3 agrees well with this prediction.

This scaling argument was also theoretically given by Milchev and Binder [13]; instead of an expression written in terms of ν, they directly used the Flory exponent $\nu = 3/5$ in the expression for $\tau_{\mathrm{rot}}(N,D)$, which yields

$$\tau_{\mathrm{rot}}(N,D) \propto N^{5/2}/D^{1/2}. \tag{10}$$

There are two important dependencies in this expression, the power-law scaling form in N and that in D. The $N^{5/2}$ dependence of the rotational time has been confirmed by Milchev and Binder [13], and later by Hagita and co-workers [14,15]. The limited range of D examined by these authors, however, could not be used to convincingly confirm the $D^{-1/2}$ dependence. Only very recently did Dimitrov and co-workers confirm the scaling form for both $\tau_{\mathrm{diff}}(N,D)$ and $\tau_{\mathrm{rot}}(N,D)$ in both N and D dependences using molecular dynamics simulations [16]. With numerical data over almost a decade of variation, our simulation data in this work have also provided concrete evidence for the confirmation of both N and D dependencies, expressed in a reduced form in Eq. (9), for both τ_{rot} and τ_{diff}.

Finally, we analyze our simulation data for the looping time τ_{loop} that the two ends of polymer take to approach each other from an open conformation. The data in Fig. 3 show that in the large N limit τ_{loop} can be well represented in a reduced form,

$$\tau_{\mathrm{loop}}(N,D)/N^{1+2\nu} \propto g(D/N^{\nu}), \tag{11}$$

which is similar to Eq. (6) for the rotational relaxation of the end-to-end distance vector. There are a few notable features in $g(x)$. As the polymer is weakly confined in the relatively large D/N^{ν} regime, the compression from the two walls reduces the mean squared end-to-end distance. This can be viewed directly from the measurement of $\langle \mathbf{R}^2 \rangle$ (not shown here) which reaches a minimum as D/N^{ν} is reduced from the large D/N^{ν} regime. Because of the closer distance between the ends in compression, the two ends find each other more easily; hence τ_{loop} is shortened in comparison with that in an unconfined space. As the distance between the walls is further reduced, the size of the polymer in the x and y directions, $\langle \mathbf{R}_{\parallel}^2 \rangle^{1/2}$, increases more rapidly than the reduction of the size in the z direction, D. The mean square distance between the two ends goes through a minimum and becomes dominated by $\langle \mathbf{R}_{\parallel}^2 \rangle$, in the strong confinement regime. Correspondingly, the looping time of the ends also goes through a minimum. The minima in these two cases occur at approximately the same location where the distance between the walls is approximately twice the free-space radius of gyration of the polymer. The fact that $\langle \mathbf{R}^2 \rangle$ contains a minimum located at a confinement distance D that is approximately double the gyration radius of an unconfined polymer has also been seen in previous studies [37,38]. The close connection between τ_{loop} and the mean square end-to-end distance is a reflection of the fact that a looping event necessitates the decline of R^2 to the prespecified value (in our work, $3l$). In comparison, the rotation time τ_{rot} is dominated by the behavior of $\langle \mathbf{R}_{\parallel}^2 \rangle$ in the entire D regime, where the latter does not go through such a minimum. See the light gray symbols in Fig. 3.

B. Tube confinement

In this section, we consider a polymer chain under the confinement of a square tube with four impenetrable walls as schematically shown in Fig. 1(b), where the axis of the tube coincides with the z axis. The characteristic confinement scale is now the size of the square tube, D. In comparison with a polymer in a slit, a polymer confined in a square tube displays a number of very different characteristic dynamic properties. As shown in Fig. 4, as functions of N and D, the three time scales that we have measured, τ_{diff}, τ_{rot}, and τ_{loop}, all approach a scaling form similar to Eq. (6). The main difference between these three times is the asymptotic behavior in the small D/N^{ν} regime.

For the diffusion time τ_{diff}, we can still take Eq. (7) for a polymer in a tube, with the understanding that $\langle \mathbf{R}_{\parallel}^2 \rangle$ is the mean square end-to-end distance in the z direction, that is, along the axis of the tube. The properties of $\langle \mathbf{R}_{\parallel}^2 \rangle$ are well understood [1,39]. We can consider the scaling law for the dimension of the elongated polymer in strong tube confinement and the fact that the polymer dimension must be proportional to N in the extreme one-dimensional limit to arrive at [2]

$$\langle \mathbf{R}_{\parallel}^2 \rangle / N^{2\nu} \propto (D/N^{\nu})^{-(2-2/\nu)}. \tag{12}$$

Hence

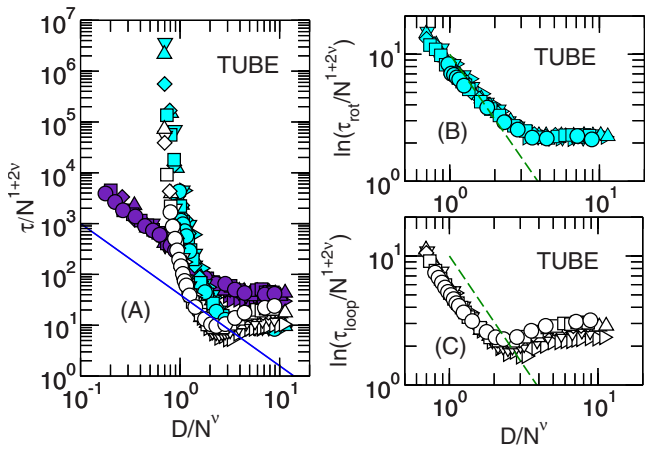

FIG. 4. (Color online) Reduced dynamic time scales as a function of D/N^{ν}, for a self-avoiding polymer confined in a square tube with a cross-section area of D^2. Open, light gray (cyan online), and dark gray (purple online) symbols represent the looping time, rotation time, and diffusion time, respectively. The solid straight line in the logarithmic plot (a) is an indication of a slope of −1.40. The dashed lines in double-logarithmic plots (b) and (c) are indications of a slope of $-1/\nu$ where $\nu=0.588$. Circles, squares, diamonds, up triangles, down triangles, and right triangles correspond to polymer chain lengths (the number of bonds) $N=199$, 99, 63, 39, 19, and 9.

$$\tau_{\rm diff}(N,D)/N^{1+2\nu} \propto (D/N^{\nu})^{-(2-2/\nu)}. \tag{13}$$

The dark gray symbols in Fig. 4(a) show that the simulation data for $\tau_{\rm diff}(N,D)$ indeed follow this scaling behavior in the small D/N^{ν} regime, where the solid line indicates a slope of $-(2-2/\nu)\approx -1.40$ in the double-logarithmic plot.

Directly using the Flory exponent $\nu=3/5$, we can write $\tau_{\rm diff}(N,D)$ in the strong confinement regime as

$$\tau_{\rm diff}(N,D) \propto N^3 D^{-4/3}, \tag{14}$$

which contains both N^3 and $D^{-4/3}$ dependencies. The N^3 dependence of the diffusion time has been previously verified by Avramova and Milchev in their Monte Carlo simulation of the diffusive motion of a polymer in strong confinement [17]. The $D^{-4/3}$ dependence, however, remained untested in their work. Our simulation data have verified both dependencies through the reduced form in Fig. 4 as displayed by Eq. (13).

The simulation results for the rotational time $\tau_{\rm rot}$ of the end-to-end vector, measured through the definition of the correlation function in Eq. (1), are displayed in Fig. 4(a) by various light gray symbols for different D and N. The open symbols in the figure represent the looping time $\tau_{\rm loop}$ when the polymer forms a ring configuration from an open configuration. We observe that, in the small D/N^{ν} regime, the numerical data for $\tau_{\rm rot}$ and $\tau_{\rm loop}$ display a very different behavior from $\tau_{\rm diff}(N,D)$.

In strong tube confinement the terminal ends of the polymer chain are normally located near the two far ends of the elongated conformation. Within the diffusion time a polymer can move from its original position by a distance comparable to the elongated size in a strong confinement. During this time, however, the two terminal ends of the confined polymer mostly stay within the same region of the overall conformation, moving along with the center of mass of the polymer. In the limit where D is much smaller than the overall length of the conformation, the decay time of the correlation function in Eq. (1) corresponds to a reversal of the end-to-end vector in the tube. An intermediate state for the reversal of the ends is a conformation where the two ends approach each other, forming a configuration similar to a ring polymer in strong tube confinement. Hence, in the small D/N^{ν} regime, the looping time and reversal time behave similarly,

$$\tau_{\rm loop}(N,D) \propto \tau_{\rm rot}(N,D). \tag{15}$$

Because looping is an intermediate state for reversal, $\tau_{\rm loop}(N,D)$ is normally lower than $\tau_{\rm rot}(N,D)$ in a narrow tube. This can also been seen from our data in Fig. 4(a).

Huang and Makarov have recently considered this transition in terms of the free energy difference between a ring polymer and a linear polymer, both having the same N and confined by tubes with the same D; to the leading order the free-energy difference can be estimated by a scaling argument, $\Delta G=CN/D^{1/\nu}$, where C is an N- and D-independent constant. This physical picture leads to a looping time

$$\tau_{\rm loop}(N,D) = \tau_0 \exp(CN/D^{1/\nu}). \tag{16}$$

The prefactor τ_0 may contain power-law factors of N and D; however, the most dominant feature is the exponentially long relaxation time, in terms of $N/D^{1/\nu}$.

To test the validity of the above equation, in Figs. 4(b) and 4(c) we have plotted $\ln[\tau_{\rm rot}(N,D)/N^{1+2\nu}]$ and $\ln[\tau_{\rm loop}(N,D)/N^{1+2\nu}]$ as functions of D/N^{ν}. Both vertical and horizontal axes have been further treated in logarithmic scale, so that the $\exp(CN/D^{1/\nu})$ dependence can be demonstrated by a linear line of the slope $-1/\nu$. Indeed, we observe that the simulation data converge this slope, represented by the dashed lines in these two plots.

The dependencies of the relaxation times on N and D, of a polymer in a tube, display different scaling laws in the strong confinement regime. One of the other most important time scales is the relaxation time of the entire conformation, which was first discussed by Hagita and Takano [40],

$$\tau_{\rm HT}(N,D) \propto N^2 D^{1/3}. \tag{17}$$

This is a much faster time scale than some of the times that we have discussed above. This relaxation time also captures the typical dynamical time for an overly stretched chain to relax from its initial nonequilibrium position. Sheng and Wang have addressed this issue and verified the Hagita-Takano power law by direct observation of the dynamics of a tube confined polymer relaxing from a nonequilibrium state to an equilibrium state [41]. This and other dynamic time scales have also been analyzed in terms of a blob picture and computer simulation data, by Arnold *et al.* recently [19].

C. Cubic pore

Finally, we discuss the dynamic times for a self avoiding polymer in a cubic pore. Figure 5 shows our simulation data for the rotation time $\tau_{\rm rot}$ of the end-to-end distance vector and the looping time $\tau_{\rm loop}$ of ends approaching each other.

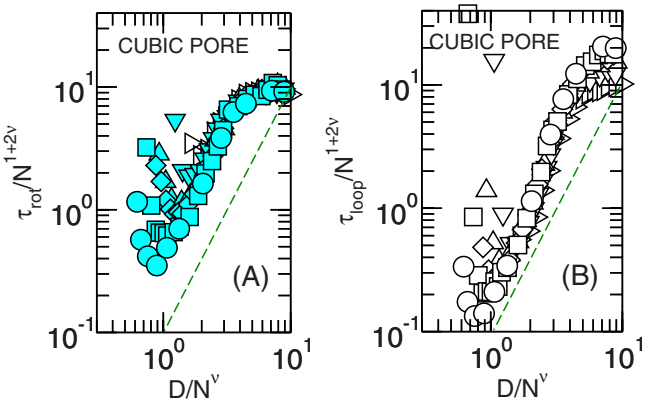

FIG. 5. (Color online) Reduced dynamic time scales as a function of D/N^{ν}, for a self-avoiding polymer confined in a cubic pore with volume D^3. Open and light gray (cyan online) symbols represent the looping time and rotation time, respectively. The dashed straight lines in the logarithmic plots are an indication of a slope of 2. Circles, squares, diamonds, up triangles, down triangles, and right triangles correspond to polymer chain lengths (the number of bonds) $N=199$, 99, 63, 39, 19, and 9.

The simulation data are represented in a reduced form by plotting $\tau_{\mathrm{rot}}(N,D)/N^{1+2\nu}$ and $\tau_{\mathrm{loop}}(N,D)/N^{1+2\nu}$ as functions of D/N^{ν}.

There are two characteristic regimes in this figure. The first is in the intermediate confinement regime where both $\tau_{\mathrm{rot}}(N,D)/N^{1+2\nu}$ and $\tau_{\mathrm{loop}}(N,D)/N^{1+2\nu}$ start to converge to a common scaling law. Because of the overall confinement, the rotation time of the end-to-end vector is similar to the diffusion time for the end-to-end vector to virtually travel a distance D. This allows us to write

$$\tau_{\mathrm{rot}}(N,D) \propto D^2/D_0. \tag{18}$$

In the intermediate confinement regime, the diffusion coefficient D_0 is not significantly different from that of a polymer in a free space and is inversely proportional to N. Then we have

$$\tau_{\mathrm{rot}}(N,D)/N^{1+2\nu} \propto (D/N^{\nu})^2. \tag{19}$$

Our simulation data points in Fig. 5 indeed approach such a scaling law (see the slope represented by the dashed line), before divergence in a smaller D/N^{ν} regime.

Strong confinement is another interesting regime in this figure, where the above scaling form breaks down. For small D, the monomer density inside the cube, N/D^3, is no longer small. We expect that any scaling behavior suitable for the description of the nondense regime breaks down when

$$D \propto N^{1/3}. \tag{20}$$

For a given N, $\tau(N,D)$ as a function of D in Fig. 5 shows a minimum where a D_{min} can be determined; this $D_{\mathrm{min}}(N)$ is also a characteristic size of the cubic pore where the scaling law in Eq. (19) breaks down. Figure 6 shows that the function $D_{\mathrm{min}}(N)$ can be well represented by the estimate in Eq. (20).

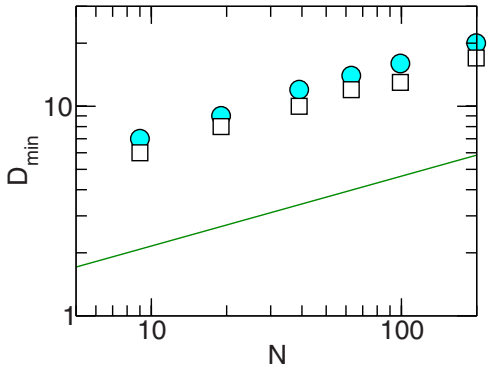

FIG. 6. (Color online) The size of a cubic pore where the rotation time and looping time show a minimum as a function of N. Gray (cyan online) and open symbols represent data determined from the minima in Figs. 5(a) and 5(b), respectively, for each given N. The solid line represents a slope of 1/3.

IV. SUMMARY

In summary, we have performed Monte Carlo simulations to investigate the characteristic dynamic times of a self-avoiding polymer confined in three types of environment: slit, tube, and cubic pores. The results have been analyzed in the light of scaling theories.

For a strong slit confinement, we have found that our data for the rotational time for the decorrelation of the end-to-end vector from its original position, the diffusion time for the displacement of the polymer center of mass to a distance equivalent to the size of the polymer, and the looping time for the two ends of the polymer to approach each other, all merge to scaling behavior similar to that of a two-dimensional self-avoiding polymer. In particular, the power law in Eq. (9) is a good representation of our simulation data, for all three dynamic time scales.

For a strong tube confinement, we have found that the simulation data for the diffusion time follow a power-law scaling behavior [Eq. (13)] and the rotation time (more exactly the reversal time) as well as the looping time can be well represented by an exponential scaling law [Eq. (16)].

For a strong cube confinement, in the relatively dilute regime before the pore size reduces to a characteristic value, the rotational and looping times can be well represented by the power law in Eq. (19). The breakdown of the scaling behavior and the onset of dynamics of a dense system can be well estimated by using the characteristic pore size represented in Eq. (20).

In all three types of confinement, weak confinement encourages the reduction of the mean square distance and hence a faster looping time. This observation is consistent with the simulation results for the intrachain binding time of a single polymer chain in a spherical box [22], and the folding time of proteins in a chaperonin cage [5] as well as in spherical pores [4].

ACKNOWLEDGMENTS

We are grateful for financial support from the NSF of China (Grants No. 50533010 and No. 20774020), the Chi-

nese Ministry of Science and Technology (973 Projects No. 2009CB930000 and No. 2005CB522700), the Chinese Ministry of Education (Key Grant No. 305004), the Science and Technology Developing Foundation of Shanghai (Grant No. 07JC14005), the Shanghai Education Committee (Project No. B112), and the NSERC of Canada. J.Z.Y.C. thanks Fudan University for making this collaboration possible and Bae-Yeun Ha for the enlightening discussion on the scaling behavior of the free energy of a polymer confined in a narrow tube.

[1] M. Daoud and P. G. de Gennes, J. Phys. (Paris) **38**, 85 (1977).
[2] P. G. de Gennes, *Scaling Concepts in Polymer Physics* (Connell University Press, Ithaca, NY, 1993).
[3] H. Zhou and K. Dill, Biochemistry **40**, 11289 (2001).
[4] D. Klimov, D. Newfield, and D. Thirumalai, Proc. Natl. Acad. Sci. U.S.A. **99**, 8019 (2002).
[5] F. Takagi, N. Koga, and S. Takada, Proc. Natl. Acad. Sci. U.S.A. **100**, 11367 (2003).
[6] M. Cheung, D. Klimov, and D. Thirumalai, Proc. Natl. Acad. Sci. U.S.A. **102**, 4753 (2005).
[7] W. Reisner, K. J. Morton, R. Riehn, Y. M. Wang, Z. Yu, M. Rosen, J. C. Sturm, S. Y. Chou, E. Frey, and R. H. Austin, Phys. Rev. Lett. **94**, 196101 (2005).
[8] C. H. Reccius, J. T. Mannion, J. D. Cross, and H. G. Craighead, Phys. Rev. Lett. **95**, 268101 (2005).
[9] M. C. Choi, C. D. Santangelo, O. Pelletier, J. H. Kim, S. Y. Kwon, Z. Wen, Y. Li, P. A. Pincus, C. R. Safinya, and M. W. Kim, Macromolecules **38**, 9882 (2005).
[10] A. Balducci, P. Mao, J. Y. Han, and P. S. Doyle, Macromolecules **39**, 6273 (2006); C. C. Hsieh, A. Balducci, and P. S. Doyle, *ibid.* **40**, 5196 (2007).
[11] P.-K. Lin, C.-C. Fu, Y.-L. Chen, Y.-R. Chen, P.-K. Wei, C. H. Kuan, and W. S. Fann, Phys. Rev. E **76**, 011806 (2007).
[12] F. Brochard and P. G. de Gennes, J. Chem. Phys. **67**, 52 (1977).
[13] A. Milchev and K. Binder, J. Phys. II **6**, 21 (1996).
[14] K. Hagita, S. Koseki, and H. Takano, J. Phys. Soc. Jpn. **68**, 2144 (1999).
[15] K. Hagita and H. Takano, J. Phys. IV **10**, 305 (2000).
[16] D. Dimitrov, A. Milchev, K. Binder, L. Klushin, and A. Skvortsov, J. Chem. Phys. **128**, 234902 (2008).
[17] K. Avramova and A. Milchev, J. Chem. Phys. **124**, 024909 (2006).
[18] F. Wagner, G. Lattanzi, and E. Frey, Phys. Rev. E **75**, 050902(R) (2007).
[19] A. Arnold, B. Bozorgui, D. Frenkel, B.-Y. Ha, and S. Jun, J. Chem. Phys. **127**, 164903 (2007).
[20] L. Huang and D. E. Makarov, J. Chem. Phys. **128**, 114903 (2008).
[21] N. Lee, C. Abrams, and A. Johner, Europhys. Lett. **72**, 922 (2005).
[22] C. Abrams, N. Lee, and A. Johner, Macromolecules **39**, 3655 (2006).
[23] I. Carmesin and K. Kremer, Macromolecules **21**, 2819 (1988).
[24] H. Deutsch and K. Binder, J. Chem. Phys. **94**, 2294 (1991).
[25] P.-Y. Lai and K. Binder, J. Chem. Phys. **95**, 9288 (1991).
[26] S. Kreitmeier, M. Wittkop, and D. Goritz, Phys. Rev. E **59**, 1982 (1999).
[27] K. Luo, T. Ala-Nissila, and S.-C. Ying, J. Chem. Phys. **124**, 034714 (2006).
[28] Y. Xie, H. Yang, H. Yu, Q. Shi, X. Wang, and J. Chen, J. Chem. Phys. **124**, 174906 (2006).
[29] T. Cui, J. Ding, and J. Z. Y. Chen, Macromolecules **39**, 5540 (2006).
[30] K. Binder, *Monte Carlo Simulation in Statistical Physics* (Springer, New York, 1988).
[31] M. E. J. Newman and G. T. Barkema, *Monte Carlo Methods in Statistical Physics* (Oxford University Press, New York, 1999).
[32] Y.-J. Sheng, J. Z. Y. Chen, and H.-K. Tsao, Macromolecules **35**, 9624 (2002).
[33] J. C. Le Guillou and J. Zinn-Justin, Phys. Rev. Lett. **39**, 95 (1977).
[34] A. Milchev and K. Binder, Eur. Phys. J. B **3**, 477 (1998).
[35] M. Doi and S. Y. Edwards, *The Theory of Polymer Dynamics* (Oxford University Press, New York, 1988).
[36] B. Nienhuis, Phys. Rev. Lett. **49**, 1062 (1982).
[37] J. H. van Vliet, M. C. Luyten, and G. ten Brinke, Macromolecules **25**, 3802 (1992).
[38] P. Cifra and T. Bleha, Macromol. Theory Simul. **8**, 603 (1999).
[39] T. W. Burkhardt and I. Guim, Phys. Rev. E **59**, 5833 (1999).
[40] K. Hagita and H. Takano, J. Phys. Soc. Jpn. **68**, 401 (1999).
[41] Y.-J. Sheng and M.-C. Wang, J. Chem. Phys. **114**, 4724 (2001).